Design and analysis of a composite beam for infrastructure applications

Part I: Preliminary investigation in bending

by

Mario Springolo[1], Gerard van Erp[2], Amar Khennane[3*]

[1,3] Faculty of Engineering and Surveying, The University of Southern Queensland, Toowoomba, Qld 4350, Australia
[2] Professor, Executive Director, Fibre Composite Design and Development Centre. The University of Southern Queensland, Toowoomba, Qld 4350, Australia

Abstract:

The objective of this study is to contribute to the development of a composite beam for use in civil engineering systems. Based on the limitations in existing concepts, a new beam design is proposed and its behaviour studied. Using the classical beam theory, the Timoshenko beam theory, the Timoshenko plate theory, as well as the transformed section approach, borrowed from reinforced concrete, a simplified analytical approach, which could be used in design, is developed to conduct first and second order analysis of the proposed beam in order to achieve a rational sizing of its section before a rigorous testing regime is carried out. Finally, to validate the analytical model and gain confidence in the design, the analytical and experimental results are compared to a rigorous non linear finite element solution. It was found that the analytical model agreed relatively well with the experiments and the FE analyses, giving confidence in the validity of the underlying assumptions.

Keywords: composite beam, design, prototype, Timoshenko beam, Timoshenko plate theory, transformed section.

*Lecturer, Faculty of Engineering and Surveying, The University of Southern Queensland, Toowoomba, Qld 4350, Australia
Tel: (+61) (7) 4631 1383, Fax: (+61) (7) 4631 2526, email: khennane@usq.edu.au

Biographical notes: Mr Mario Springolo received his PhD in February 2005 from the Faculty of Engineering and Surveying at USQ. He is currently working as a structural engineer with Larken Teys consulting Pty Ltd. http://www.larkinteys.com.au

Biographical notes: Professor Van Erp was born and educated in the Netherlands and moved to Asutralia in 1989. In 1990 he joined the Faculty of Engineering and Surveying at USQ. Currently, he is the Executive Director of Fibre Composites Design & Development, University of Southern Queensland (USQ) responsible of Australia's first fibre composites bridge.

Biographical notes: Dr Amar Khennane holds a BE from Tizi-Ouzou, Algeria, an M.Sc. from Heriot Watt, UK, and a PhD, from UQ, Australia. Before joining the Faculty of Engineering and Surveying at the University of Southern Queensland, he was a researcher with the Cooperative Research Centre for Advanced Composite Structures, Ltd, Australia. His research interests are in composite materials: micro-mechanics, durability and through life estimation of composite structures, and computational mechanics.

INTRODUCTION

Fibre Reinforced Polymers (FRP) offer potential qualities such as light weight, high stiffness-to-weight and strength-to-weight ratios, ease of installation in the field, potentially lower systems level cost, and potentially high overall durability, which makes them attractive for incorporation into civil engineering systems. However, the high performance attributes of FRP are yet to be fully realised by the civil engineering community. Indeed, the use of composites in the infrastructure industry is relatively recent, and there is a lack of an "experience of use" basis. The development of codes and guidelines to meet the needed performance criteria is necessary to contribute to the wider acceptance of composites by the infrastructure industry. Further research is therefore needed into the behaviour and design of composite structural elements. The work presented in this study could be viewed as a contribution to this area. It addresses the development and analysis of the behaviour under load of a beam prototype. In this part and the subsequent one, anisotropy is not taken into account as they deal with preliminary design. However, anisotropy may be important, and it is considered in details in the third part of the paper, which presents the nonlinear finite element analysis of the beam.

NEW BEAM PROTOTYPE

Traditional FRP beams whose cross sections mimic steel sections are known to fail long before the ultimate load-carrying capacity of the reinforcing fibres is achieved. It is therefore apparent from existing designs that limited engineering has been used in the development of composite beams. This is particularly noticeable for some early commercially available pultruded sections where the advantage of mass production overshadowed quality. These early pultruded beams were characterised by a large number of premature failures such as delamination at internal corners, compression flange buckling, and web buckling. Since then,

the pultruted process has come a long way, but some problems inherent to the orientation of the fibres still remain. The other commercial process used to produce FRP beams is filament winding. Because of inherent geometric limitations this process is not well suited for the manufacture of beams. Sections must be uniform, fibre orientation is restricted, with the optimum zero degree in the flanges being unobtainable, and the shape of the beam can have no reverse curvature. Custom designed beams have been proposed to address these shortcomings albeit with mixed success. The most successful are those that combine FRP with a core material, such as concrete [1,2]. These concrete filled beams appear to have solved many problems. However, unless using stay-in-place forms, the bonding of the concrete to the FRP has emerged as a major deficiency of this concept. Replacement of cementious concrete with polymer concrete appears to be a solution [3]. The beam prototype proposed herein uses this technology. A new beam design whose main purpose is to avoid the aforementioned early failure modes in a cost-effective manner is being developed at the Fibre Composite Development and Design Centre (FCDD), University of Southern Queensland, Australia. The beam prototype is shown on Figure 1. Table 1 and Table 2 show respectively the materials properties of the laminates, and their dimensions of the cross section of the beam. The E-Glass reinforcement was kindly donated by Colan Pty. Ltd, Australia.

The incorporation of a core material made of Particulate Filled Resin (PFR), composed by mass of 70 % resin and 30% mix of fly ash micro-spheres of a range of sphere sizes between 150 and 300 microns in diameter, not only provides restraints against flange buckling but also constitutes an effective solution to web buckling by enhancing the structural stability and reducing bearing pressures across the web. To reduce dead weight and the overall cost of the beam the core material is placed between web laminate layers, thus making the webs and flanges efficient sandwich structures with the laminates located where the highest strains are

likely to occur. The role of the two FRP RHS (Rectangular Hollow Sections), one inside the other, is to confine the core material, which is placed within. They also contribute to the shear and torsional stiffness of the beam. The fibres in the RHS laminates are placed at ±45 degrees with respect to the longitudinal axis in order to enhance the resistance of the section when subject to shear and torsion of the section. The flanges have an extra layer of reinforcement with fibres aligned, with the longitudinal axis, positioned inside the outer RHS to provide resistance to compressive and tensile forces induced by bending moments. The webs are similar to the flanges, and extra laminates, with an optimum orientation at ±45 degrees to the longitudinal axis of the beam, can also be provided within the core to provide extra shear resistance.

However, if the dimensions of the beam are poorly chosen in the preliminary design, secondary failure modes may still occur, or excessive quantity of materials used. Therefore, a simplified method of analysis is required so that the test beams can be designed and a testing program developed. To develop such a method, formulas from classical beam theory and thin walled beam theory, coupled with the transformed section analysis, will be adjusted to allow for laminate properties. The formulas will identify the critical parameters that govern the different failure modes of the new beam. To allow for cracking of the core material, a method similar to that commonly used in reinforced concrete analysis is adopted so that load – deflection curves can be generated. In addition to these simplifying assumptions, the anisotropy in the laminates, interplay debonding, and fibre rupture have been totally neglected in the preliminary design method, but will be taken into account in the subsequent finite element analysis.

PRIMARY FAILURE MODES IN BENDING

Moment curvature behaviour

The behaviour of an FRP beam incorporating PFR is somewhat similar to that of a reinforced concrete (RC) beam. Indeed, the PFR is somehow similar to a cementious material in both appearance and behaviour. As shown on Figure 2, the FRP beam progresses through an initial linear elastic segment (region 1) before cracking of the core material, which results in a reduction in stiffness (region 2). With increasing load, the stiffness continues to deteriorate. However, unlike a well designed RC beams, there is no tangible 'yield plateau' because of the linear-elastic behaviour of the glass reinforcement. Therefore, the beam continues to sustain increasing load until it ultimately fails (point 3).

In the linear-elastic range, the beam behaviour is well described by the moment-curvature relationship. That is:

$$\kappa = \frac{M}{EI} \tag{1}$$

where: κ is the curvature of the beam, M is the moment, and EI is the stiffness. As is common for reinforced concrete beams, a similar expression can be also used for the cracked stage of the FRP beam (region 2):

$$\kappa = \frac{M}{EI_{effective}} \tag{2}$$

where $EI_{effective}$ lies between $EI_{un\text{-}cracked}$ and $EI_{cracked}$. In order to derive an expression for $EI_{effective}$ it is useful to determine these upper and lower boundaries first.

To account for the different materials in the cross-section, the transformed section approach is used [4]. The transformed section for the un-cracked FRP beam, together with the strain and stress distributions are represented on Figure 3. The dissimilar width of the core material in

the compression zone, relative to that in the tensile zone, is related to the different moduli of elasticity of FRP and PFR in compression and tension. As a result, the stress distribution throughout the FRP beam's cross-section is not linear, as shown on Figure 3d. It is therefore easier to describe the behaviour of the individual laminates in terms of strain:

$$\varepsilon_{(y)} = \frac{My}{EI} \tag{3}$$

where $\varepsilon_{(y)}$ is the strain at a distance y from the neutral axis, and I and E are respectively the second moment of area and reference modulus of the transformed section. By comparing the strains throughout the cross section against the core material capacity, it can be determined when cracking is likely to occur.

However, equation (3) must be used iteratively as the tensile behaviour of the PFR is non-linear as shown on Figures 4 and 5. In tension the curve corresponding to the PFR behaviour with constant area is exactly the same as the curve inclusive of Poisson's effect, and only the later one appears on Figure 3. Based on the calculated tensile modulus of elasticity, the transformed section is updated at each iteration.

Cracking of the core material has a significant influence on the overall stiffness and failure performance of the FRP beam. For the purpose of developing a simplified method of analysis, a crack is assumed to initiate first at the interface between the bottom laminate and the core material when a limiting strain criterion is violated. Once it is formed, the laminates become the principal tensile load-carrying element at that location. The exact behaviour of this process, and its influence on strength and stiffness is very complex. As with RC beams, analysis can be simplified significantly by disregarding any tensile contribution of the core material to the strength and stiffness at the position of a crack. The transformed section at the position of a crack is shown on Figure 6. For the sake of clarity, the stress contribution of the

web laminates is omitted from Figure 6. By ignoring the tensile capacity of the core material, the neutral axis shifts up the beam, and the overall stiffness at that location is reduced.

Effective stiffness of the beam

Once the limiting strain is exceeded, a number of cracks develop along the length of the beam with increasing moment. This progressive formation of cracks reduces the beams' effective stiffness, $EI_{effective}$, which decreases from the un-cracked state, $EI_{un\text{-}cracked}$, towards the fully cracked state, $EI_{cracked}$. However, the stiffness will always remain slightly higher than $EI_{cracked}$ because the beam is a composite of cracked and un-cracked segments. Given the similarity of this behaviour with that of a RC beam, the approach developed by Kordina and Quast [5] is adopted to predict estimates for the effective stiffness of the FRP beam. This approach assumes the moment-curvature relationship to be bi-linear. The effective stiffness is obtained as the slope of the curve in the cracked region.

Assuming that the ultimate failure of the FRP beam is caused by tensile laminate rupture, the bilinear approximation can be used to express the effective stiffness in terms of tensile strains as:

$$EI_{effective} = EI_{un-cracked} - \left(EI_{un-cracked} - EI_{cracked}\right)\frac{\left(\varepsilon_t - \varepsilon_{ft12}\right)}{\left(\varepsilon_{ft13} - \varepsilon_{ft12}\right)} \quad (4)$$

Therefore, the effective distance to the neutral axis corresponds to:

$$c_{effective} = c_{un-cracked} + \left(c_{cracked} - c_{un-cracked}\right)\frac{\left(\varepsilon_t - \varepsilon_{ft12}\right)}{\left(\varepsilon_{ft13} - \varepsilon_{ft12}\right)} \quad (5)$$

where: ε_{ft12} and ε_{ft13} are respectively the tensile failure strains of the core L_{12} and laminate L_{13} as shown in the cross section on Figure 1, and ε_t is the highest tensile strain in the core material at a given load. Equations (4) and (5) completely describe the moment-curvature relationship of the beam.

Primary failure modes

The unidirectional laminates (L_2 and L_{13}) are the stiffest elements within the beam, and they withstand the majority of the resultant tensile and compressive forces generated by the applied bending moment. The rupture of any of these laminates will cause the total collapse of the beam, as the remaining materials are incapable of absorbing the released energy. Consequently, the two primary failure modes of the beam are either tensile or compressive failure of the unidirectional laminates. Due to the characteristics of these laminates, both these failure modes are brittle in nature, and they occur at the locations of highest strain. The point of highest strain in the laminate happens at the location of a previously formed crack in the PFR. The tensile failure of the bottom unidirectional laminate (L_{13}) creates a hinge in the beam, which therefore becomes a mechanism. When the strain distribution through the depth of the beam is assumed to be linear, the curvature at failure can be expressed as:

$$\kappa = \frac{\varepsilon_{ft13}}{c_{cracked} - t_{14}} \tag{6}$$

where $c_{cracked}$ is the distance from the bottom of the beam to the neutral axis, and t_{14} is the thickness of the bottom exterior RHS laminate. Substitution of equation (6) into equation (1) results in the following expression for the failure moment, M_f:

$$M_f = \frac{\varepsilon_{ft13} EI_{cracked}}{c_{cracked} - t_{14}} \tag{7}$$

In the compressive zone, the compressive force imposed on the section is shared between all the materials above the neutral axis. The unidirectional laminate, *L2*, has the lowest failure strain of all these materials. Its failure is accompanied by the total collapse of the beam. The failure moment can be expressed as:

$$M_f = \frac{\varepsilon_{fc2} EI_{cracked}}{D - c - t_1} \tag{8}$$

where: ε_{fc2} is the compressive failure strain of the unidirectional laminate, D is the depth of the beam, t_1 is the thickness of the top outer RHS laminate, and the effect of the PFR is encompassed within $EI_{cracked}$.

Predominant primary failure mode

The materials within the beam have compressive moduli that are higher than their respective tensile moduli. This, coupled with the core cracking, causes the neutral axis of the beam to rise. Due to this shift in neutral axis, the tensile strains are higher than their respective compressive strains. Furthermore, the unidirectional laminates have a higher failure strain in compression than in tension. As a result, tensile failure will always be predominant. Therefore, the amount of tensile unidirectional laminate is the critical parameter governing primary failure. However, if a very small amount of tensile reinforcement is provided, tensile failure may occur immediately after the first crack in the core material [6]. To avoid such premature failure, in a static loading regime, sufficient tensile laminate should be provided so that $M_f >> M_{cracked}$.

SECONDARY FAILURE MODES IN BENDING

A range of secondary failure modes may precede the aforementioned primary failure modes. In many instances, the predominant cause of these secondary failure modes is the lack of sufficient web and flange restraint.

The beam section is comprised of flanges and relatively thin webs surrounding a void. Due to this geometry, moment buckling of the webs and compression buckling of the top flange may occur. In addition, increased curvature of the beam induces compressive forces in the webs.

Similar forces also occur at locations where the beam is externally loaded or supported. Associated with these forces are the following failure modes identified on Figure 7:

(a) compression buckling of the webs;

(b) crushing of the webs;

(c) tearing of the web laminates;

(d) laminate failure in the flanges;

(e) punching shear of the core in the flanges; and

(f) longitudinal cracking of the core in the flanges.

Potentially, any of these failure modes could precede the primary failure mode discussed before. Due to the complex boundary conditions and the resulting multidimensional stress states within the beam's cross section, the failure loads are difficult to predict. However, using standard linear-elastic thin-walled beam theory, approximate solutions and the key parameters governing such failures can be obtained.

Moment buckling of the webs

As represented on Figure 7, compressive and tensile stresses are induced in the relatively thin webs. The compressive stresses may cause localised buckling of the web, which results in a reduced effective stiffness of the web and, therefore precipitating the failure of the beam. The rigidity of the connection between the web and the flanges has a major influence on the magnitude of the buckling load. In the case of the present FRP beam, the core material at the web-flange interface may crack, resulting in a boundary condition similar to a hinge. Therefore, treating this boundary as hinged is appropriate. Its analytical treatment is based upon formulations developed for flat plates [7]. When these formulae are adopted for the sandwich structure of the web under consideration, they result in:

$$\sigma_{mb.cr} = \frac{k_2 \pi^2 E}{12\left(1-\nu_w{}^2\right)}\left(\frac{t_w}{d_b}\right)^2 \tag{9}$$

where: E is the reference modulus of the transformed section, ν_w is the Poisson ratio of the entire web [8], t_w is the thickness of the web, and d_b is the depth of the void in the FRP beam. The coefficient k_2 equals 23.8 for simple supports. Using Hooke's law, expression (9) can be altered so that the critical moment buckling strain is expressed as:

$$\varepsilon_{mb.cr} = \frac{23.8\pi^2}{12\left(1-\nu_w{}^2\right)}\left(\frac{t_w}{d_b}\right)^2 \tag{10}$$

From this equation, it is apparent that the web thickness, t_w, has a major impact upon buckling capacity.

At any given moment, the compressive strain in the web can be calculated by substituting the relevant dimensions into equation (3) as follows:

$$\varepsilon_{mb} = \left(D - c - \sum_{i=1}^{4} t_i\right)\frac{M}{EI_{effective}} \tag{11}$$

To determine whether moment buckling of the web is likely, the results of equations (10) and (11) are compared. The onset of web moment buckling can be expected if $\varepsilon_{mb} \geq \varepsilon_{mb.cr}$. If moment buckling precipitates primary failure of the beam, extra core material can be added to increase t_w and thereby increase the buckling capacity of the web.

Compression buckling of the top flange

Under pure bending, the top flange of the beam is subjected to uniform compression. In the case of a relatively thin top flange, this may result in localised buckling that reduces the stiffness of the beam and causing the neutral axis to move towards the tension flange. The result of this shift is an increase in compressive strain in the buckled flange, and therefore accelerating failure of the beam. To palliate against this failure mode, core material is added to the flanges of the beam. However, this failure may still occur if the thickness of core

material is insufficient. To identify the key parameters for the flange buckling resistance, the buckling capacity of the flange needs to be estimated.

The asymmetry of the flanges adds further complication to the analysis. By ignoring this asymmetry, the theory of plate buckling can be extended to the loading condition of flange compression buckling. Using the same rationale as for moment buckling of the webs, simply supported edge conditions were assumed herein. This results in exactly the same form as equation (9) for critical compression buckling stress [9] with a k_2 equalling 4 for simply supported edges. The critical buckling strain for the sandwich panel flange then becomes:

$$\varepsilon_{cb.cr} = \frac{4\pi^2}{12\left(1-\nu_f{}^2\right)}\left(\frac{t_f}{W-2t_w}\right)^2 \tag{12}$$

where: ν_f is the Poisson ratio of the flange [8], t_f is the thickness of the flange, and W is the width of the beam. From equation (12), it is apparent that web and flange thickness are key parameters. Of these two, flange thickness has a dominant influence upon the buckling strain.

The strain of the compression flange can be calculated by substituting the relevant dimensions into equation (3) as follows:

$$\varepsilon_1 = \frac{M\left(D-c\right)}{EI} \tag{13}$$

The onset of flange buckling can be expected if $\varepsilon_1 \geq \varepsilon_{cb.cr}$.

Failure of the RHS laminate within the flanges

High values of the bending moment in the flanges could result in the failure of the RHS laminate and the core material, which in turn may cause the beam to split along its longitudinal axis. In addition, the associated shear forces could also cause the unidirectional laminate to punch into the void of the beam.

The resulting transverse strains in laminates L_1 and L_4 are proportional to the thickness of the flange, and can be calculated per unit length of beam, using equation (3), as follows:

$$\varepsilon_{1(x)} = \frac{-M_{(x)}\left(t_f - c_f\right)}{EI_f} \tag{14}$$

and

$$\varepsilon_{4(x)} = \frac{M_{(x)}c_f}{EI_f} \tag{15}$$

where: t_f is the thickness of the flange, c_f is the distance from the bottom of the flange to the neutral axis of the flange, and EI_f is the stiffness of the flange (in the transverse direction). These estimated strains are compared with the capacities of the laminates L_1 and L_4 to determine whether failure is likely. Since the PFR material has a lower tensile failure strain than the laminates, it is expected to fail first.

Additional failure modes due to bearing loads

In addition to moment buckling, possible failure modes such as crushing, or tearing of the webs, can also occur under vertical compression forces in the webs generated by an externally applied bearing load, Figure 8, or by the curvature in the beam as represented on Figure 9.

The presence of the force F_w may place the webs in a state of lateral instability, which can result in their crushing or tearing. Increasing core thickness results in a higher buckling capacity. Part of the force F_w is transferred to the webs through the core material. As a result, the web is also subjected to shear and flexure. The transverse shear stress in the core resulting from the curvature of the beam can be calculated as follows:

$$\tau_{xy3(x)} = \frac{F_w\left(\frac{1}{2} - \frac{x}{W}\right)}{t_{3(x)}} \tag{16}$$

Where $t_{3(x)}$ represents flange thickness at x.

Additional shear stresses caused by external bearing plate loading can be calculated as follows:

$$\tau_{xy3} = \frac{F_w}{2t_3} \text{ for } 0 \le x \le a \text{ and } \tau_{xy3} = 0 \text{ for } x > a \tag{17}$$

where *a* is the distance from the edge of the beam to the location of load contact as shown on Figure 10.

The critical shear stress in the core material occurs at the web-flange interface. Since the core material has been assumed isotropic, the principal strains within can be determined using Mohr's circle:

$$\varepsilon_{11,22} = \frac{\varepsilon_x + \varepsilon_y}{2} \pm \sqrt{\left(\frac{\varepsilon_x - \varepsilon_y}{2}\right)^2 + \left(\frac{\tau_{xy3}}{2G_3}\right)^2} \tag{18}$$

where: ε_x are calculated using equation (15), ε_y is taken as zero, and G_3 is the shear modulus of the PFR. From equations (15) and (17) it is apparent that the thickness of the flange is a major factor that governs the principal strain calculated in equations (14) to (18).

The calculated values can then be checked against the failure strain of the PFR to estimate when failure is likely to happen. An initial crack in the core reduces the shear area and amplifies the shear stresses as calculated in equation (16) leading to an accelerated overall failure of the flange.

CONCLUSION

Based on the transformed section approach commonly used to study the behaviour of reinforced concrete beams and the thin walled plate theory, a simplified approach is developed to study the bending behaviour of a composite beam incorporating a core material and predict its failure behaviour.

The resulting formulation revealed that the primary failure mode of the beam would be through the tensile rupture of the tensile rupture of the unidirectional reinforcement in the bottom flange. However, if the section is not properly designed, the thin walled plate theory revealed that secondary failure modes that include moment buckling of the webs, compression buckling of the top flange, compression buckling of the webs, crushing of the webs, tearing of the web laminates, laminate failure in the flanges, punching shear of the core in the flanges, and longitudinal cracking of the core in the flanges are also possible. It was found that these secondary failure modes have all one parameter in common: core thickness. As a result, they all can be averted by the judicious placement of the core material within the flanges and webs, leaving the beam to fail in the aforementioned primary tensile failure mode.

Finally, the proposed approach was used as a design tool to dimension the cross section of the beams used in a testing program whose results are presented in part III of this paper.

REFERENCES

1. Deskovic, N. Meier U., and Triantafillou, T.C. Innovative design of FRP combined with concrete: Short term behaviour. ASCE Journal of Structural Engineering, Vol.121 (7), pp 1069-1077.

2. Deskovic, N. Meier U., and Triantafillou, T.C. Innovative design of FRP combined with concrete: Long term behaviour. ASCE Journal of Structural Engineering, Vol.121 (7), pp 1079-1089.
3. Ayers SR, Van Erp, G.M. The development of a new structural core material for composites in civil engineering - Constituent influences on stiffness behaviour. International SAMPE Symposium and Exhibition (Proceedings), 2001 (46I): 427-438
4. Warner RF, Rangan BV, Hall AS. Reinforced concrete. 3rd Edn, Longman Australia Pty Ltd. 1989.
5. Kordina K, Quast U. Bemessung von schlanken Bauteilen -Knicksicheirheitsnachweis (Design of slender reinforced concrete members -stability check). Beton-Kalender, Berlin. 1971.
6. Van Erp GM. A new fibre composite beam for civil engineering applications. Advanced Composites Letters 8 (5): 219-225 1999
7. Timoshenko, S. Theory of plates and shells. 2nd Edition, McGraw Hill, New-York 1959
8. Springolo, M. New fibre-reinforced polymer box beam: investigation of static behaviour. PhD thesis. Faculty of Engineering, The University of Southern Queensland, Australia. 2005.
   http://adt.usq.edu.au/adt-QUSQ/public/adt-QUSQ20050421.122411/
9. Bulson, PS. The Stability of Flat Plates. Chatto & Windus, London. 1970

Table 1: Laminate properties

Name		**Unidirectional**		**Plain weave**
Code		*MU4500K127*		*AF251*
Density (kg/m^3)		1740		1510
Thickness (mm)		0.56		0.17
Direction		11	22	11 and 22
Tensile	*Failure stress (MPa)*	516.4 (69.3)	47.1 (3.88)	169.6 (38.4)
	Failure strain (%)	1.965 (0.154)	1.11 (0.725)	1.475 (0.106)
	Modulus (MPa)	26705 (1808)	9894 (1990)	11502 (910.9)
Compressive	*Failure stress (MPa)*	448.1 (62.7)	127.0 (20.89)	263.0 (38.8)
	Failure strain (%)	1.65 (0.235)	2.47 (0.654)	1.920 (0.126)
	Modulus (MPa)	33363 (2990)	10184 (1746)	13700 (141.5)
Shear	*Failure stress (MPa)*	47.2 (3.95)		50.2 (1.55)
	Failure strain (%)	1.39 (0.02)		2.5 (0.059)
	Modulus (MPa)	3009 (107.5)		2017 (36.71)
Poisson ratio, (ν_{12})		0.27		0.24

Table 2: Nominal dimensions of the beam cross section

Cross section	*Dimensions (mm)*	*Number of Laminates*
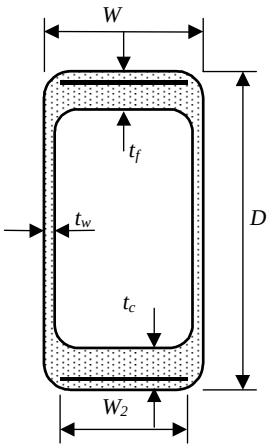	$D = 65$ $W = 33$ $w_2 = 23$ $L_3 = L_{12} = 7.5$ $L_6 = L_9 = 2.5$ $t_f = 11.76$ $t_c = 11.76$ $t_w = 3.18$	$L_1 = L_{14} = 1$ $L_2 = L_{13} = 7$ $L_4 = L_{11} = 1$ $L_5 = L_{10} = 2$ $L_7 = L_8 = 2$

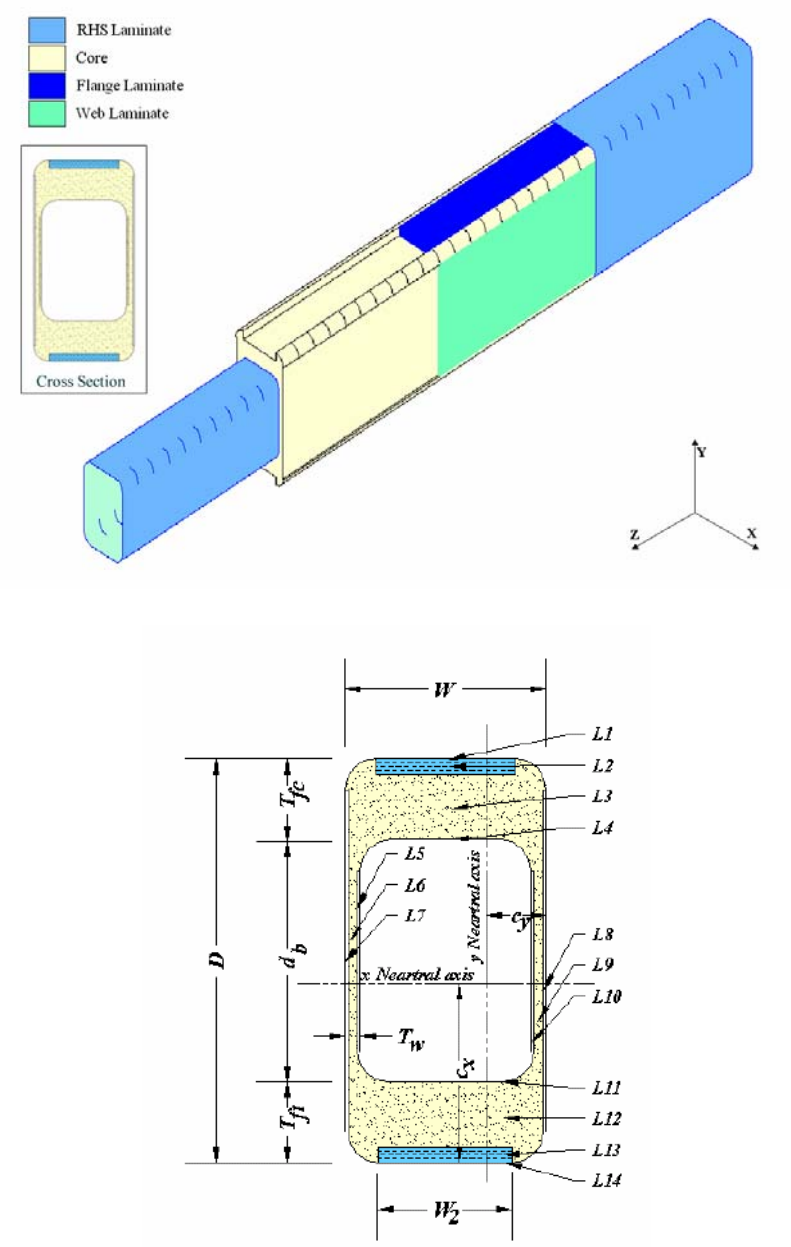

Figure 1: Three dimensional view and cross section of the beam prototype

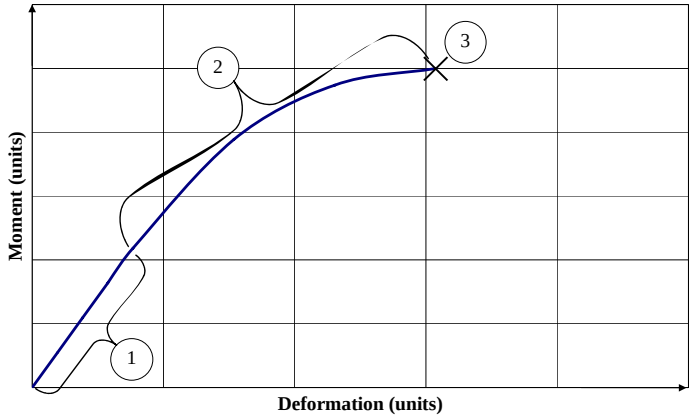

Figure 2: load deformation behaviour of a composite beam incorporating core material

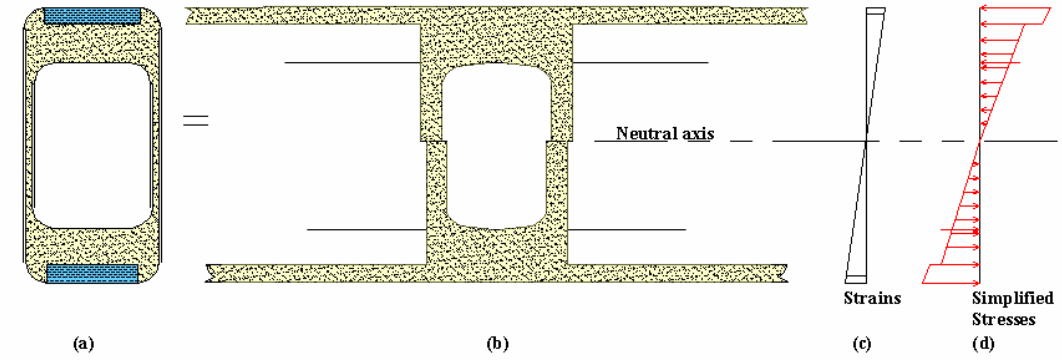

Figure 3: Transformed section of the un-cracked FRP beam

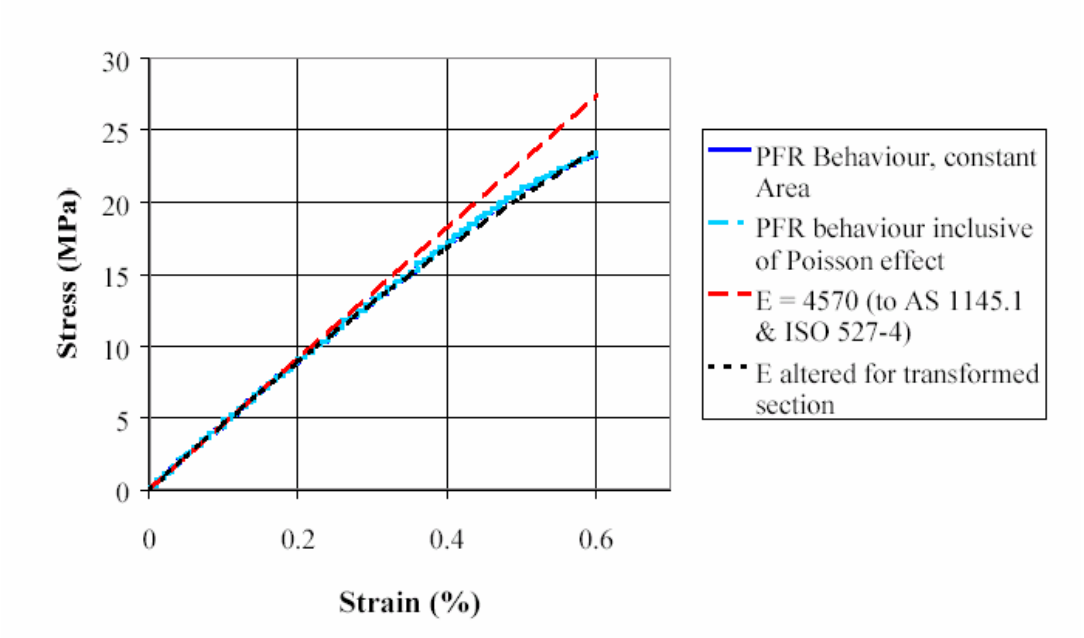

Figure 4: Stress-strain behaviour of the PFR material in tension

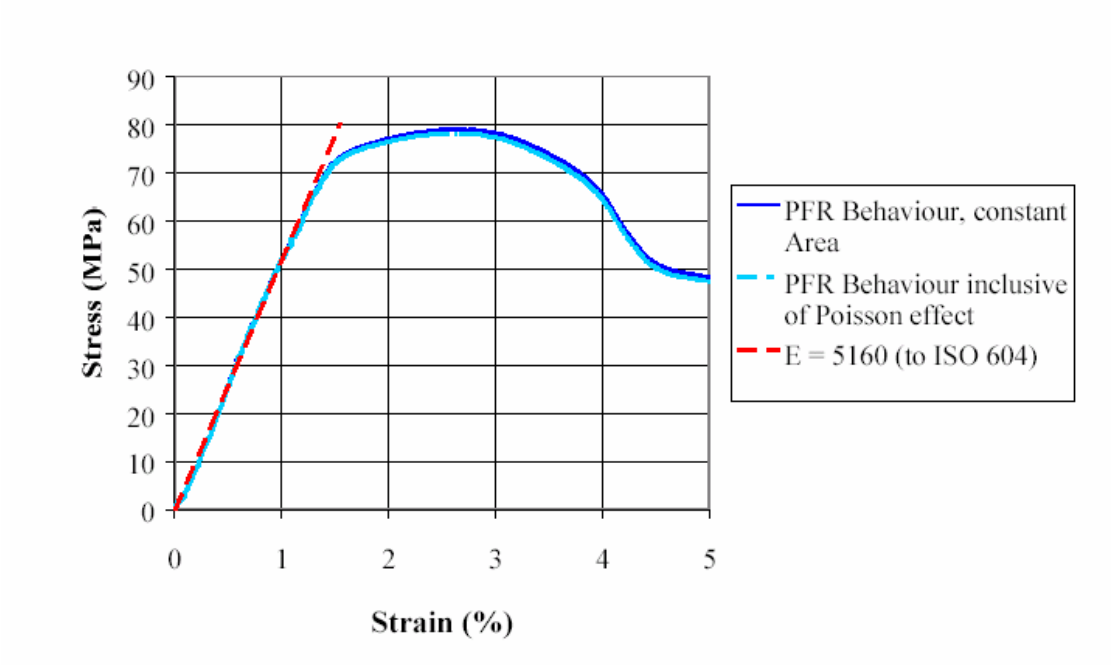

Figure 5: Stress-strain behaviour of the PFR material in compression

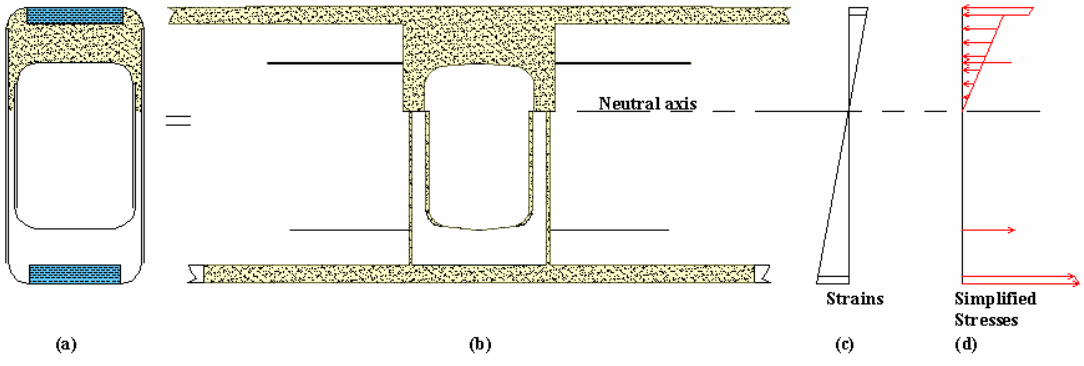

Figure 6: Transformed section of cracked FRP beam

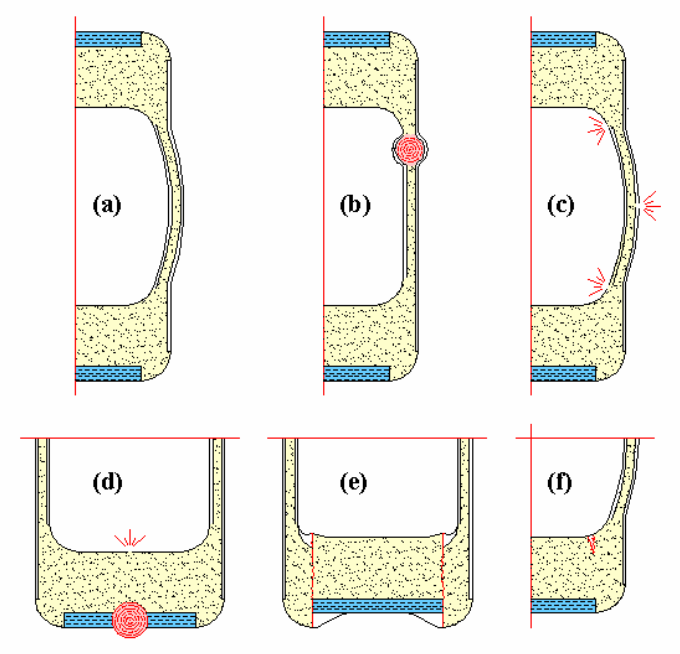

Figure 7: Some secondary failure modes in bearing

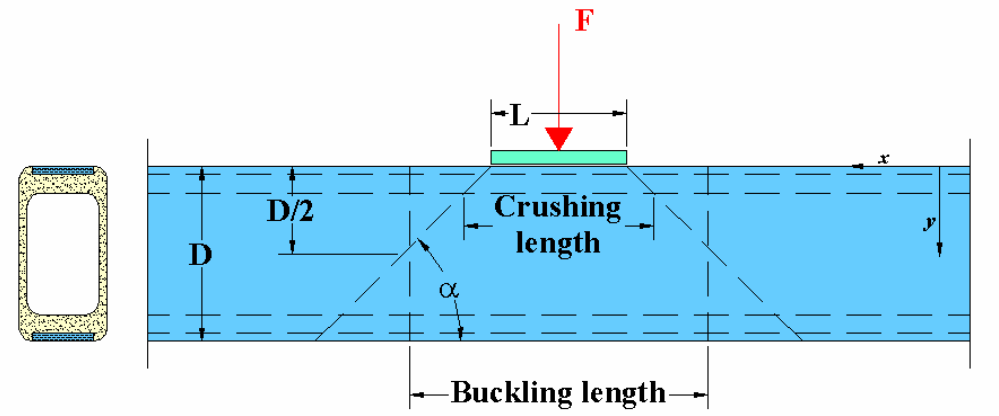

Figure 8: Vertical compression forces in the webs generated by an externally applied load

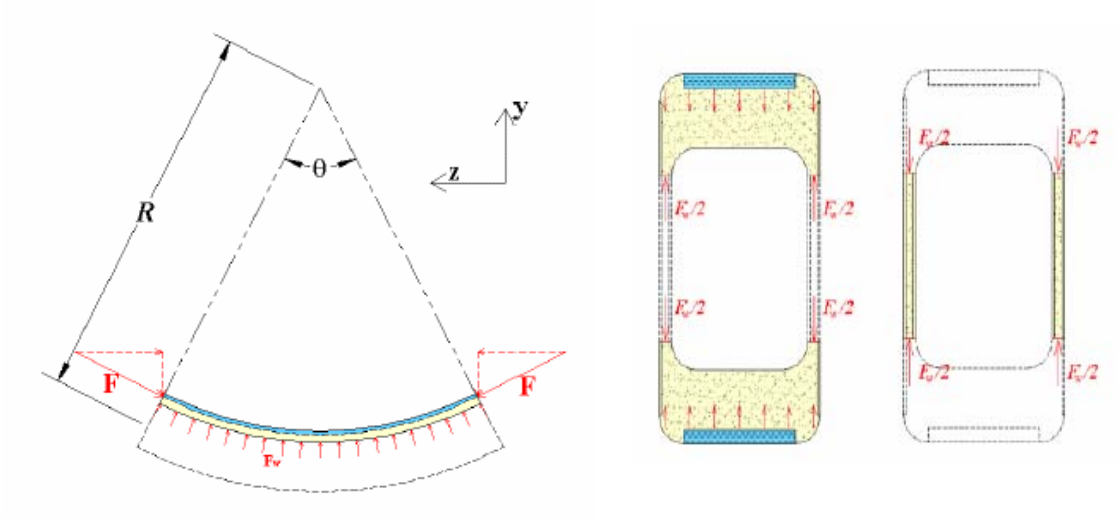

Figure 9: Secondary forces in webs induced by bending or applied external force

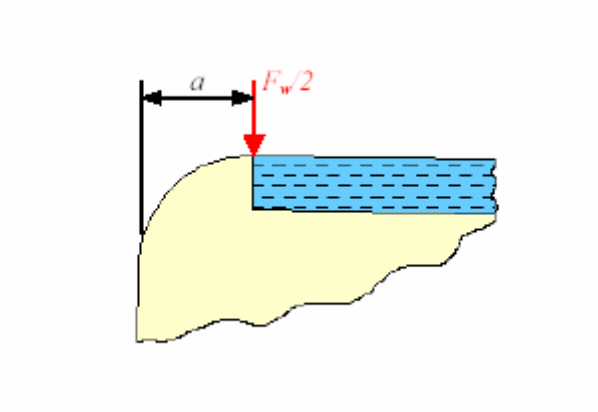

Figure 10: Significance of the parameter *a*